J MATER RES TECHNOL. 2020;9(5):11918–11934

Available online at www.sciencedirect.com

jmr&t
Journal of Materials Research and Technology
https://www.journals.elsevier.com/journal-of-materials-research-and-technology

Review Article

A review of microstructure and texture evolution with nanoscale precipitates for copper alloys

Yongfeng Geng [a,b,c,d,1], Yijie Ban [a,b,c,1], Bingjie Wang [f,1], Xu Li [d], Kexing Song [a,b,c,*], Yi Zhang [a,b,c,*], Yanlin Jia [e], Baohong Tian [a,b,c], Yong Liu [a,b,c], Alex A. Volinsky [g]

[a] School of Materials Science and Engineering, Henan University of Science and Technology, Luoyang 471023, PR China
[b] Provincial and Ministerial Co-construction of Collaborative Innovation Center for Non-ferrous Metal New Materials and Advanced Processing Technology, Henan Province, Luoyang 471023, PR China
[c] Henan Province Key Laboratory of Nonferrous Materials Science and Processing Technology, Luoyang 471023, PR China
[d] Center for Advanced Measurement Science, National Institute of Metrology, Beijing 100029, PR China
[e] College of Materials Science and Engineering, Central South University, Changsha, 410083, PR China
[f] School of Materials Science and Engineering, Southeast University, Nanjing, 210000, PR China
[g] Department of Mechanical Engineering, University of South Florida, Tampa, 33620, USA

ARTICLE INFO

Article history:
Received 4 June 2020
Accepted 12 August 2020

Keywords:
Copper alloy
Texture evolution
Microstructure evolution
Nanoscale precipitates

ABSTRACT

Copper alloys are widely used in the lead frame, high-speed railway and other applications due to their high electrical conductivity and adequate mechanical properties. In this work, the texture and microstructure evolution under hot deformation of Cu-Ni-Si, Cu-Co-Si and Cu-Fe-P alloys were investigated. In order to analyze the texture evolution, the standard pole figures and ODF figures were established. The TEM analysis shows that the addition of trace elements promoted the dispersion of nanoscale precipitated phase particles in the matrix, which can hinder the movement of grain boundaries and dislocations. In addition, the suitable hot processing parameters for the Cu-Fe-P alloy were determined from the hot working diagram. Finally, the comprehensive diagrams for the effects of addition of the alloying elements on the electrical conductivity and ultimate tensile strength of the Cu-Ni-Si and Cu-Fe-P alloys were obtained.

1. Introduction

Copper alloys are favored due to their high conductivity and excellent mechanical properties [1–7], and are widely used in aerospace, high-speed railway, home appliances, lead frames and so on [8–13]. The application diagram of copper alloys is shown in Fig. 1. Typical characteristics of pure copper are high conductivity, excellent ductility and low strength, which narrows its applications [14]. In order to improve the mechanical properties of the copper, many researchers tried adding alloying elements, such as Co [10,15,16], Al [17–19], Mg [20–22],

* *Corresponding author.*
E-mails: kxsong@haust.edu.cn, kxsong123@163.com (K. Song), zhshgu436@163.com, yizhang@haust.edu.cn (Y. Zhang).
[1] These authors contributed equally to this work.
https://doi.org/10.1016/j.jmrt.2020.08.055

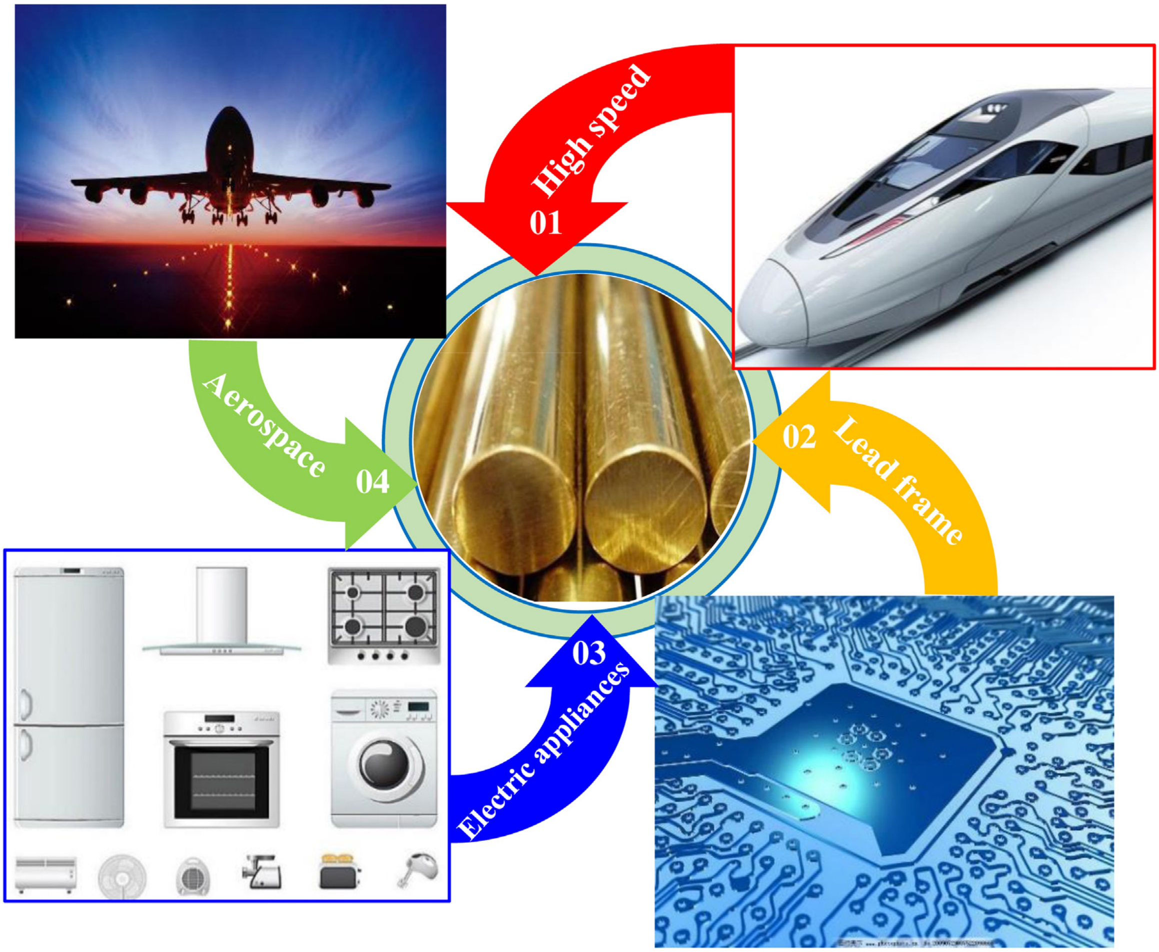

Fig. 1 – The application diagram of copper alloys.

Fe [23–25], Ti [26–29], Ag [30–32], Cr [33–35], Zr [36–38]. Good results have been achieved, demonstrating that the addition of trace alloy elements can refine grains, delay the recrystallization process, and improve the strength and hardness of of copper alloys. In the past few decades, commonly used copper alloys include Cu-Ni-Si [39,40], Cu-Ni-Al [41,42], Cu-Cr-Zr [43,44], Cu-Mg [45,46] and so on. Ni and Si can form Ni_2Si intermetallic compounds in copper alloys, and the solubility of Ni_2Si in copper matrix decreases sharply with the decrease of temperature, which has a strong precipitation strengthening effect. Ni and Al can form NiAl or Ni_2Al in copper alloys, which have strong precipitation strengthening effects at 450–600 °C. The addition of Cr and Zr produces the intermetallic compounds, which improve the strength, heat resistance and electrical conductivity of copper alloys. Lei et al. [47] obtained a high strength of Cu-Ni-Si alloy by the combined cold rolling and aging process with a peak aging performance of 381 HV (hardness), 1155.8 MPa (ultimate strength), 3.5% (elongation), and 25.2%IACS (electrical conductivity). Chalon et al. [48] investigated the flow stress, work-hardening and work-softening behavior of the Cu-Ni-Si alloy deformed at 600~950 °C. The hot working of this alloy should be carried out at temperatures higher than 850 °C, so as to obtain full benefits from the grain refinement effect due to DRX (dynamic recrystallization). Fu et al. [49] investigated the transformation of microstructure and properties in Cu-Cr-Zr alloy during cold deformation and aging processes. The results showed that plasticity is closely related to texture transformation and precipitation of large amount of Cr particles, increasing the electrical conductivity and strength. Shen et al. [50] developed a new process of hot rolling and intermediate annealing with high strength and electrical conductivity in Cu-Cr-Zr alloy. High strength and conductivity may be attributed to the fine grains and rapid precipitation of secondary phases. With the rapid development of the technology and modern economy, higher performance requirements of copper alloy are put forward, especially for those used for lead frames and high-speed railways. Therefore, researchers have been trying to add rare earth elements, such as Ce [51,52] and Y [53,54], to improve the copper alloys properties. Wang et al. [46,51] investigated the hot deformation behavior of Cu-Mg alloy with Ce and Y addition. The addition of Ce and Y significantly increased the flow stress, and activation energy for hot deformation, while it inhibited the dynamic recrystallization of the alloy, attributed to promoting precipitation and increasing number of twins after deformation.

The processing technology of copper alloys mainly includes hot deformation and aging after cold deformation. Hot deformation is a basic component of heat treatment and is widely used to investigate the hot working properties of copper

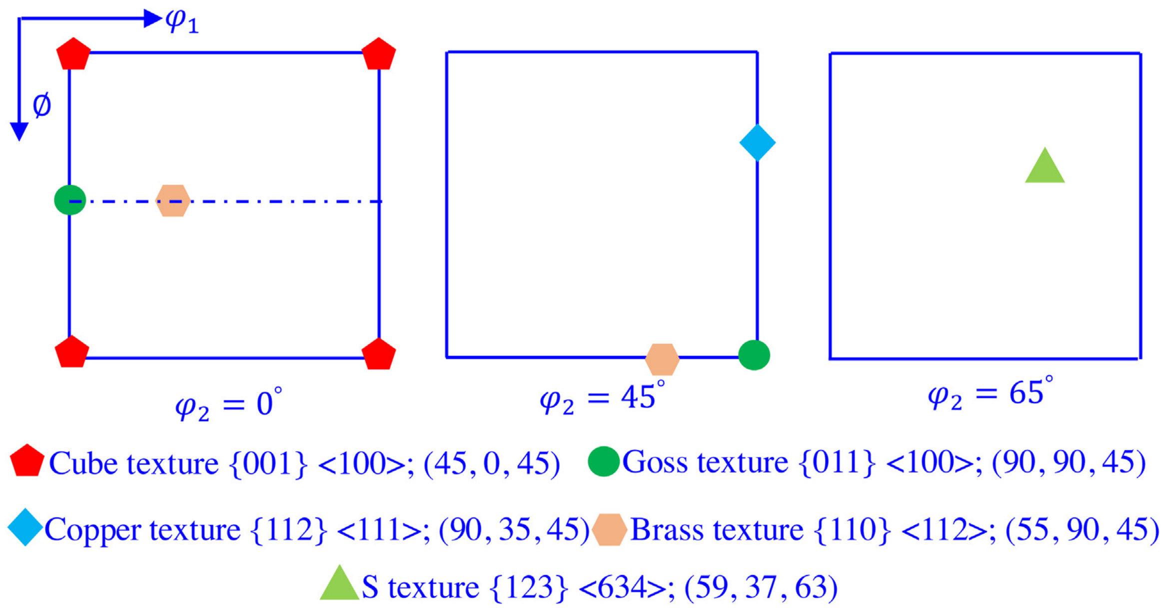

Fig. 2 – Schematic illustration of the ideal texture components for copper alloy, ODF maps at $\varphi_2 = 0°$, 45° and 65°.

alloys. Generally speaking, the hot deformation temperature and deformation rate are the main parameters that affect the hot deformation behavior of the copper alloys. Studying microstructure transformations, thermal activation energy and hot processing maps can be used to obtain the optimal deformation parameters for the hot working performance of copper alloys. Especially for the electron backscatter diffraction (EBSD) analysis obtained by the JSM-7800 F backscatter scanning electron microscope, it plays a more and more important role in the analysis of hot deformation, which can be used to analyze the microstructure and orientation of solid crystal materials under various processing conditions. In face-centered cubic (FCC) materials, the deformation process is usually accompanied by the development of unique microstructure and significant crystal texture. Especially, the development of texture during deformation is very important to control the anisotropy of mechanical properties, so it is necessary to understand the texture correctly [55]. Due to the varying orientations of grains in polycrystalline metals, the occurrence time and number of slip in grains are different, the strength of interaction between dislocations is also different, the distribution of orientation difference in crystal is certain to be different, and the deformation structure is also different. Therefore, the polycrystalline metals deformation should be inhomogeneous, and this difference has different effects on the subsequent dynamic recrystallization or phase transformation, which can be easily detected by EBSD. Moreover, the texture transformation is closely related to the properties of the alloys after heat treatment, which can be obtained from the EBSD. For FCC Metals, the main textures include {001} <100> cubic texture, the {011} <100> Goss texture, {112} <111> copper texture, {111} <211 > R texture and so on [56,57]. There are many factors that affect texture transformation during deformation, such as processing parameters and material parameters [58]. Among them, the starting grain size and strain path are the two important process parameters that have a significant influence on the microstructure and texture [59]. Bhattacharjee et al. [60] investigated the effects of starting grain size (36 μm and 800 μm) on the evolution of texture in nickel during the cross-rolling process. The results show that the significant difference in the texture was much stronger Brass ({011} <112 >) and rotated Brass ({011} <744 >) components in the fine grained starting material compared to the coarse grained starting material. It can be attributed to the different grain refinement behavior due to the large initial grain size, which is closely related to the dispersed and fragmented structure formed in the material. The change of strain path during cold rolling has a significant effect on the evolution of deformation texture, which has the characteristic of rotating 90° around the normal direction (ND) between consecutive passes so that the transverse direction (TD) of the previous rolling pass becomes the rolling direction (RD) of the current rolling pass [58,59,61]. The cross rolling processes are in sharp contrast to conventional or unidirectional routes, where RD remains constant throughout the process. Cross rolling has great influence on the formation of microstructure and texture during deformation and annealing, which has been extensively investigated in FCC materials [60,62–64]. Bhattacharjee et al. [61] reported the effects of change in strain path during cold rolling on the evolution of microstructure and texture. It was found that the copper-type texture was observed in unidirectional processed materials, while the strong brass texture was developed during cross rolling. The important material parameter which can have a significant impact on microstructure and texture is stacking fault energy (SFE) [58,60]. Brass texture is observed with the dominant component of Brass component in low SFE materials. While pure metal or copper-type texture, which are characterized by the strong Cu, S, and Brass components, can be observed in high to medium SFE materials, such as Ni and Cu [61,65]. It is especially pointed out that the addition of alloying elements will reduce the SFE of copper alloys [66]. Moreover, the addition of alloying elements

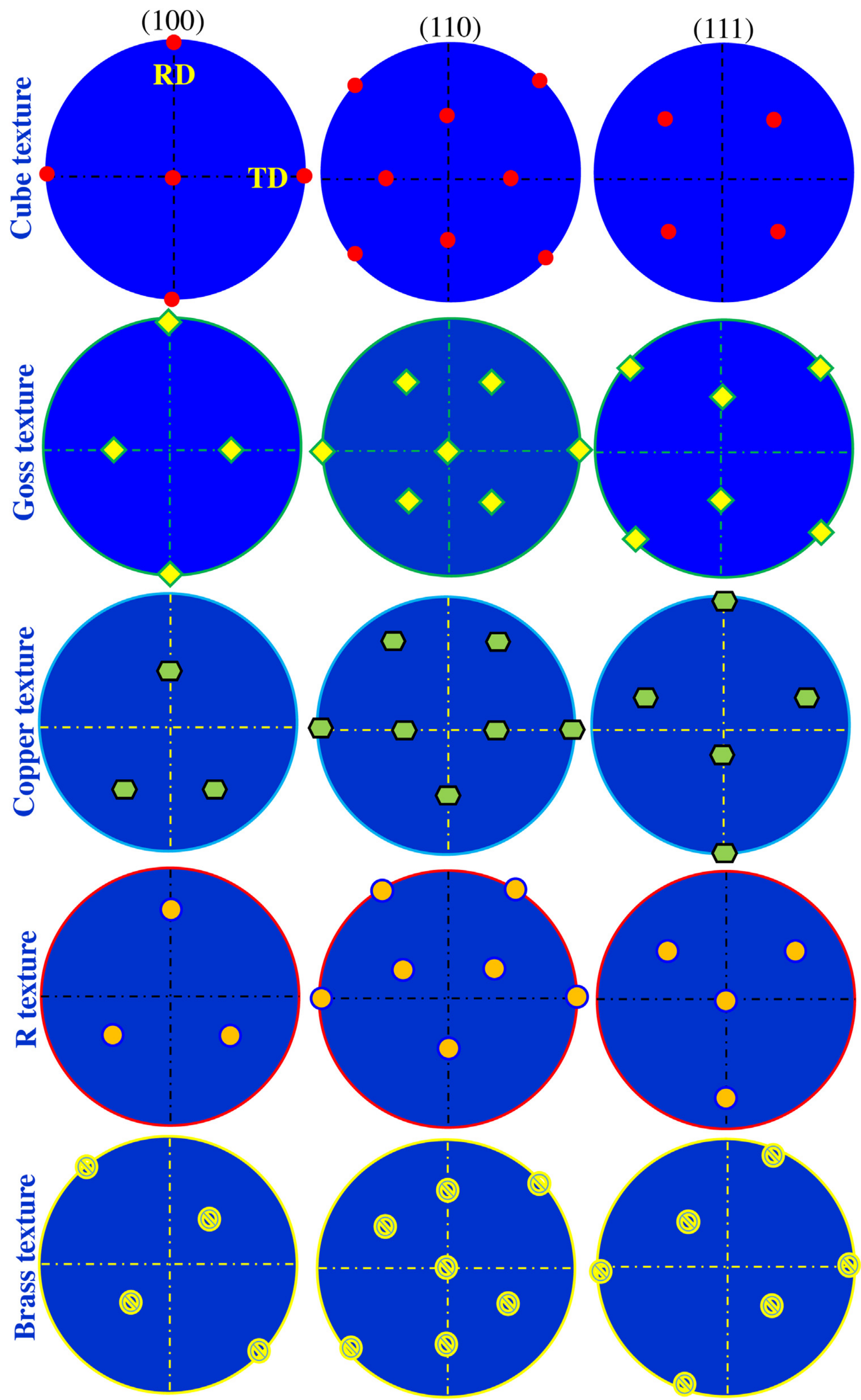

Fig. 3 – Schematic illustration of the ideal texture components for copper alloy at (100), (110) and (111) standard pole figures.

has a certain influence on the deformation and recrystallization texture. For example, it is known to significantly affect strength of the recrystallization texture in high to medium SFE materials. The results analyzed by Ray and Bhattacharjee [67] indicated that the W and Mo addition developed a much sharper cube texture compared with pure Ni. Besides, W and Mo enhance the cube texture intensity in Ni by decreasing the volume fraction of the rotated cube grains.

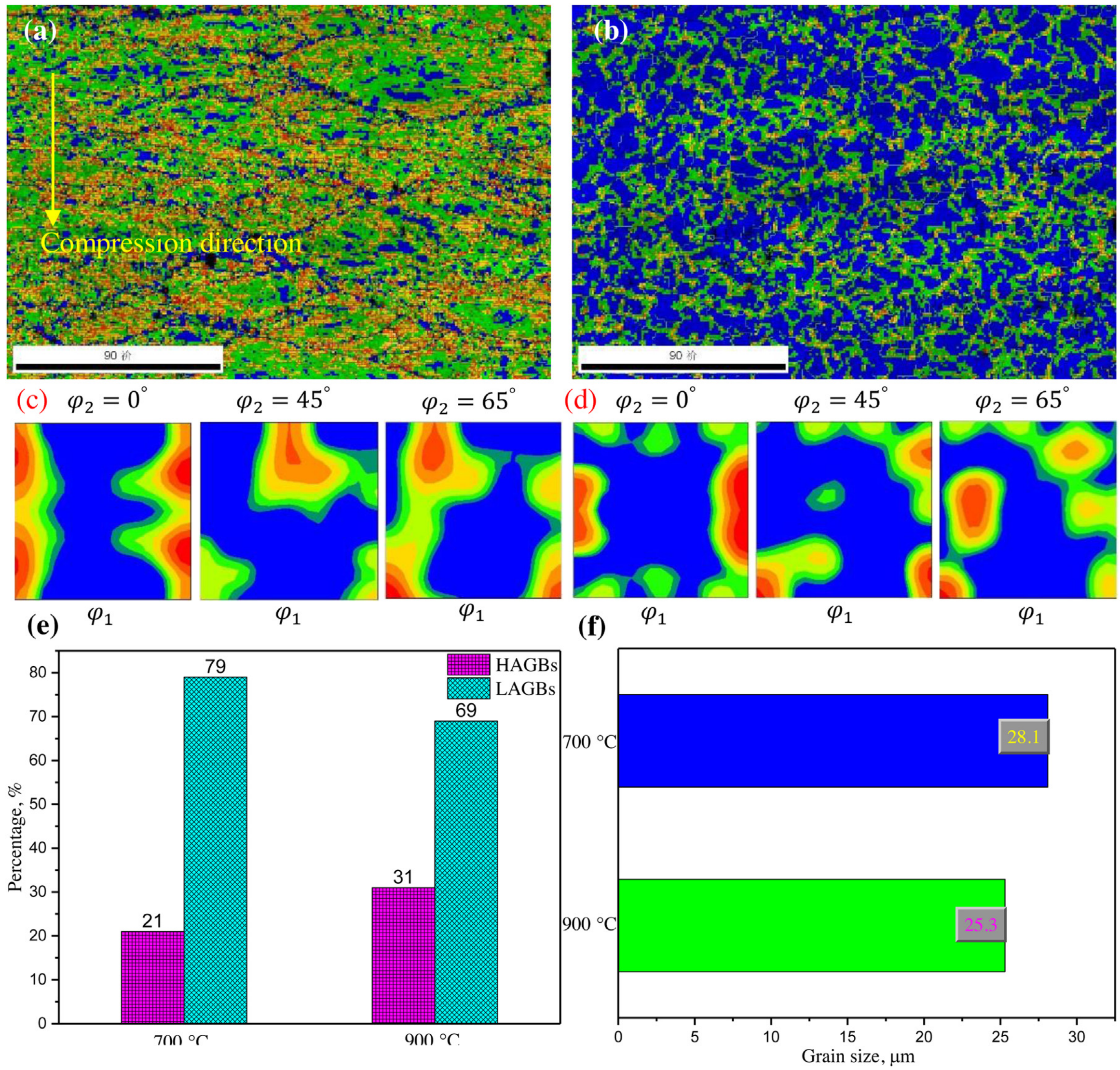

Fig. 4 – EBSD maps of Cu-Ni- Si alloy: (a) KAM map deformed at 0.01 s^{-1} and 700 °C; (b) KAM map deformed at 0.01 s^{-1} and 900 °C; (c) ODF map of (a); (d) ODF map of (b); (e) HAGBs and LAGBs percentage deformed at 700 °C and 900 °C; (f) corresponding average grain size deformed at 700 °C and 900 °C.

The cold deformation, aging temperature and time are direct factors that affecting the properties of age-strengthened copper alloys. The nanoscale precipitates in the aging process result in the high conductivity and strength of copper alloys. The combined process of cold deformation and aging for copper alloys with a small amount of alloying elements can greatly improve the hardness and tensile properties of the copper alloy due to the high dislocation density and fine precipitates, although the conductivity is slightly sacrificed. Therefore, understanding and optimizing the aging process is an important factor to control the precipitation of secondary phases to improve the properties of copper alloys [68]. In this work, several typical copper alloys (Cu-Ni-Si, Cu-Co-Si, and Cu-Fe-P) were analyzed, especially for the EBSD analysis, microstructure evolution and nanoscale precipitates.

2. Cu-Ni-Si alloy

Although Cu-Be alloy has high conductivity (~22%IACS) and strength (~1000 MPa), it has been almost replaced by the Cu-Ni-Si alloy in recent decades due to its harmful effect on human health [47,69–71]. A large amount of research reports show that when the content of Ni and Si is high, the alloy has high strength but low conductivity, which can be used as elastic conductive spring and other elastic conductive materials [72–75]. When the content of Ni and Si is low, the copper alloys have high conductivity and strength, and can be used as the lead frame materials [76–81].

The microstructure transformation during hot deformation is an important index to evaluate the hot working properties and dynamic recrystallization characteristics. In

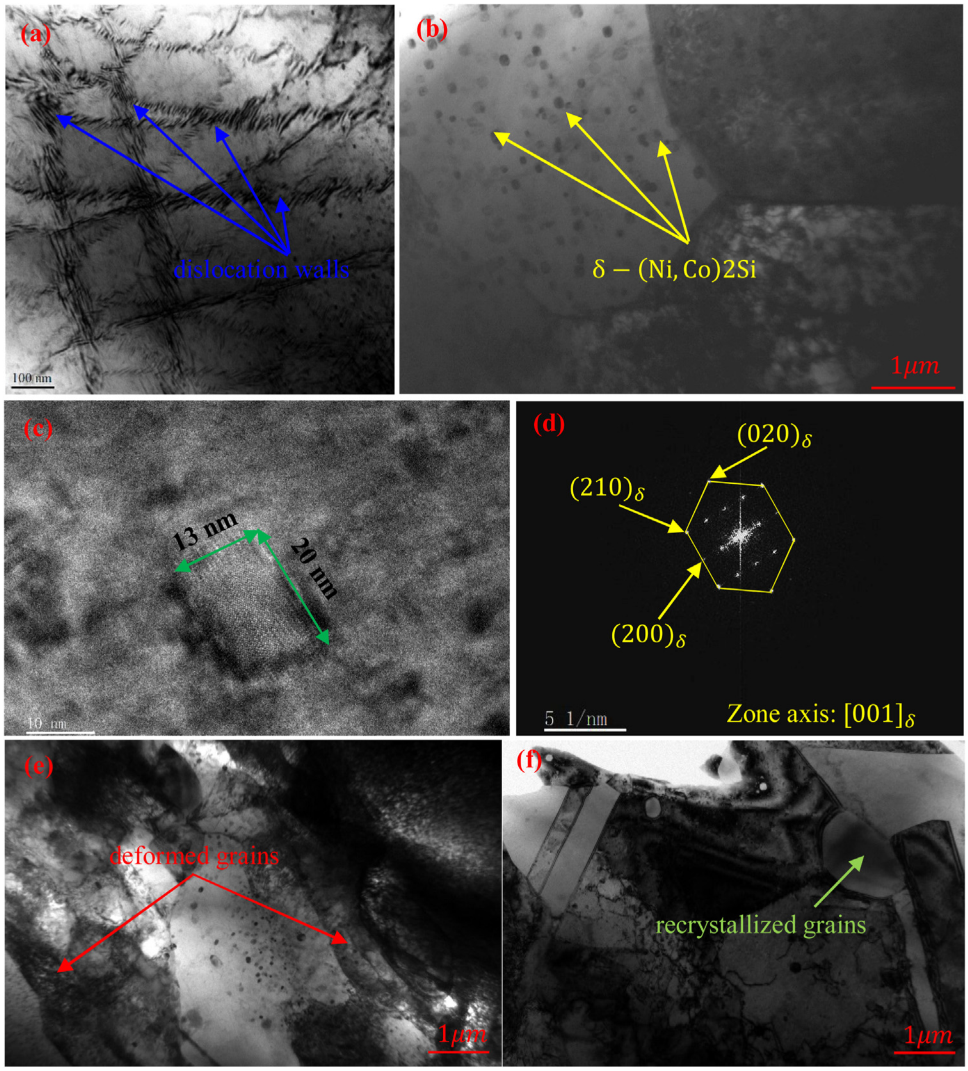

Fig. 5 – TEM micrographs of Cu-Ni-Si alloy deformed at 0.01 s^{-1} and 700 °C: (a), (b), (e) and (f) bright field images; (c) HRTEM of (b); (d) FFT of (c).

addition, the texture is closely related to the hot working properties of the copper alloy. Fig. 2 shows a schematic illustration of the ideal texture components for copper alloy according to the ODF maps at $\varphi_2 = 0°$, 45° and 65° and the Euler angles of corresponding texture. In addition, Fig. 3 shows the schematic illustration of the ideal texture components for copper alloy at (100), (110) and (111) standard pole figures.

Fig. 4 shows the EBSD maps and corresponding ODF maps, misorientation angle and average grain size of the Cu-Ni-Si alloy deformed at 0.01 s^{-1} with different temperature of 700 °C and 900 °C. As illustrated in the Fig. 4(a), there are a lot of deformed grains and a few recrystallized grains (indexed by blue color) around the deformed grains in the structure. With the increasing of deformation temperature, the number of dynamic recrystallized grains increases significantly, the deformed grains are replaced by recrystallized grains, and the microstructure is more uniform. In addition, the average grain size decreased from 28.1 μm to 25.3 μm, which is attributed to the transformation of deformed grains into recrystallized grains due to the acceleration of dynamic recrystallization. The black area in Fig. 4(a) indicates that the unindexed black area has higher lattice distortion than the indexed area [82]. It is also shown that the deformation energy at low temperature is higher than that at high temperature compared Fig. 4(a) with (b). The driving force of dynamic recrystallization is the stored energy related to dislocations during deformation, which will be released when dynamic recrystallization occurs. This can explain why the dynamic recrystallization accelerates with the increasing of temperature. In addition, the diffusion of atoms is also one of the reasons for the acceleration of dynamic recrystallization with the increasing of temperature. It can be inferred that Fig. 4(c) and (d) are the {001} <100> cubic texture and the {011} <100> Goss texture, respectively, by comparing the standard ODF maps in Fig. 2. Moreover, the texture tends to strengthen with the increasing of temperature. The first step of dynamic recrystallization is to form some crystal nuclei in the deformed matrix, which are surrounded by a large angle interface and have a high degree of structural integrity. The nucleus then grows by swallowing the surrounding matrix until the whole matrix is filled with

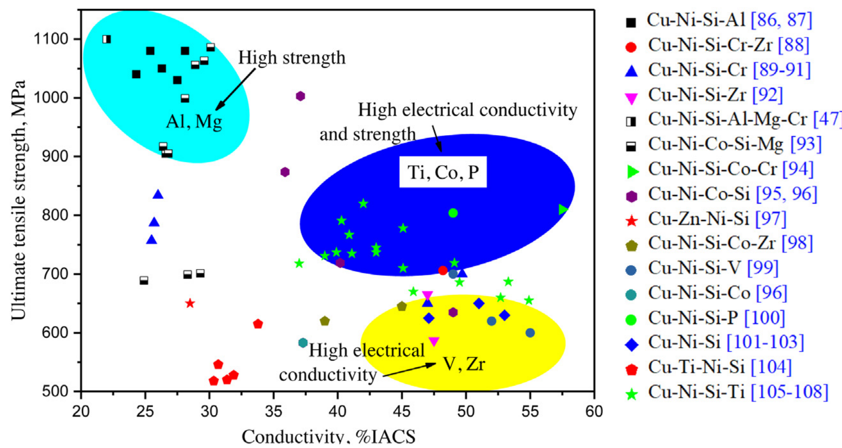

Fig. 6 – The comprehensive properties of the Cu-Ni-Si alloy with different types of alloy elements [47,86–108].

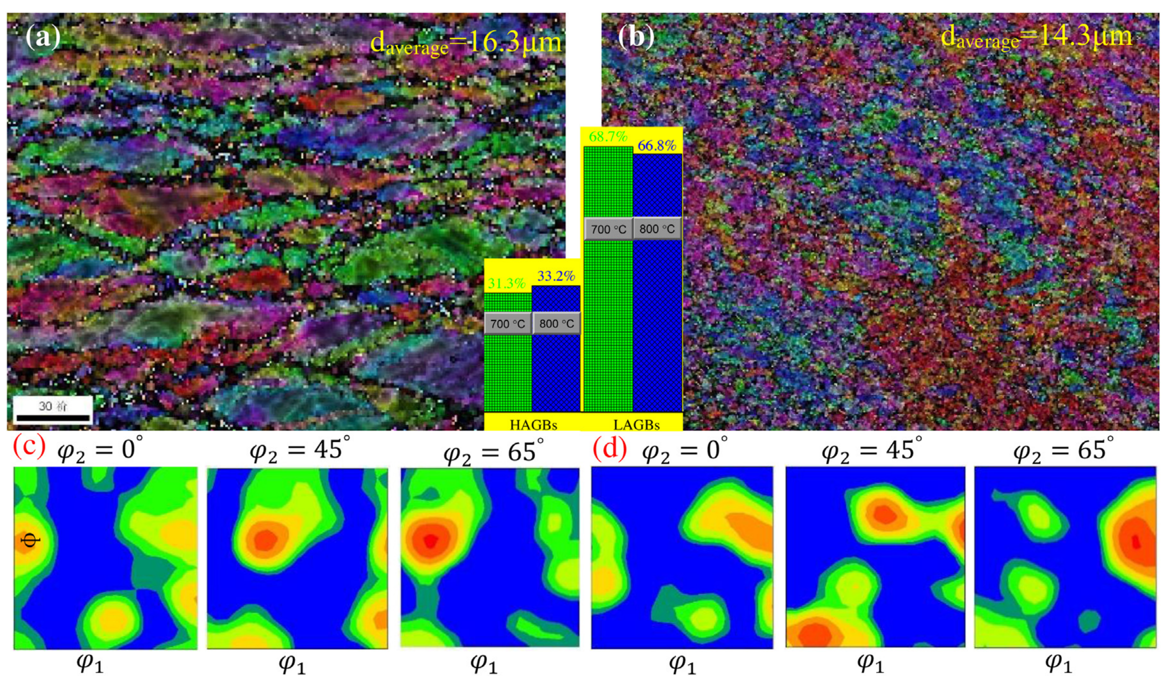

Fig. 7 – Microstructure of Cu-Co-Si-Ti alloy: (a) KAM map deformed at 700 °C and 0.01 s^{-1}; (b) KAM map deformed at 800 °C and 0.01 s^{-1}; (c) ODF map of (a); (d) ODF of (b);

new grains. The necessary conditions for the recrystallization nucleus is that they can engulf the surrounding matrix in the way of interface movement and form new grains of a certain size. Therefore, only the sub crystal with a large angle interface with the matrix can become a potential recrystallization nucleus. In other words, the content of dynamic recrystallization grain can be qualitatively inferred from the content of large angle grain boundary. Generally speaking, the recrystallization nucleation usually takes priority at the original grain boundaries, near the inclusion base surfaces, at the deformation zones and the edge cutting zones. As given in the Fig. 4(e), it shows the HAGBs and LAGBs of Cu-Ni-Si alloy deformed at 700 °C and 900 °C. It can be seen that the percentage content of HAGBs increases with the increasing of temperature, which can also prove that the degree of dynamic recrystallization increases with the increasing of temperature based on the above analysis [83–85].

Fig. 5 shows the TEM micrographs of Cu-Ni-Si alloy deformed at 0.01 s^{-1} and 700 °C. It can be seen that there are many dislocation walls and nanoscale precipitates with the size of 13 nm × 20 nm inside the grains. The existence of dislocation walls can hinder the migration of grain boundaries and make the deformation more difficult. The precipitates can be determined to be δ-(Ni, Co)$_2$Si according to the diffraction pattern in Fig. 5(d). In addition, the zone axis of δ-(Ni, Co)$_2$Si can be calculated as $[001]_δ$. Ban et al. [35] investigated the effects of Cr addition on the constitutive equation and precipitated phases of copper alloy by the ESBD and TEM analysis. It can

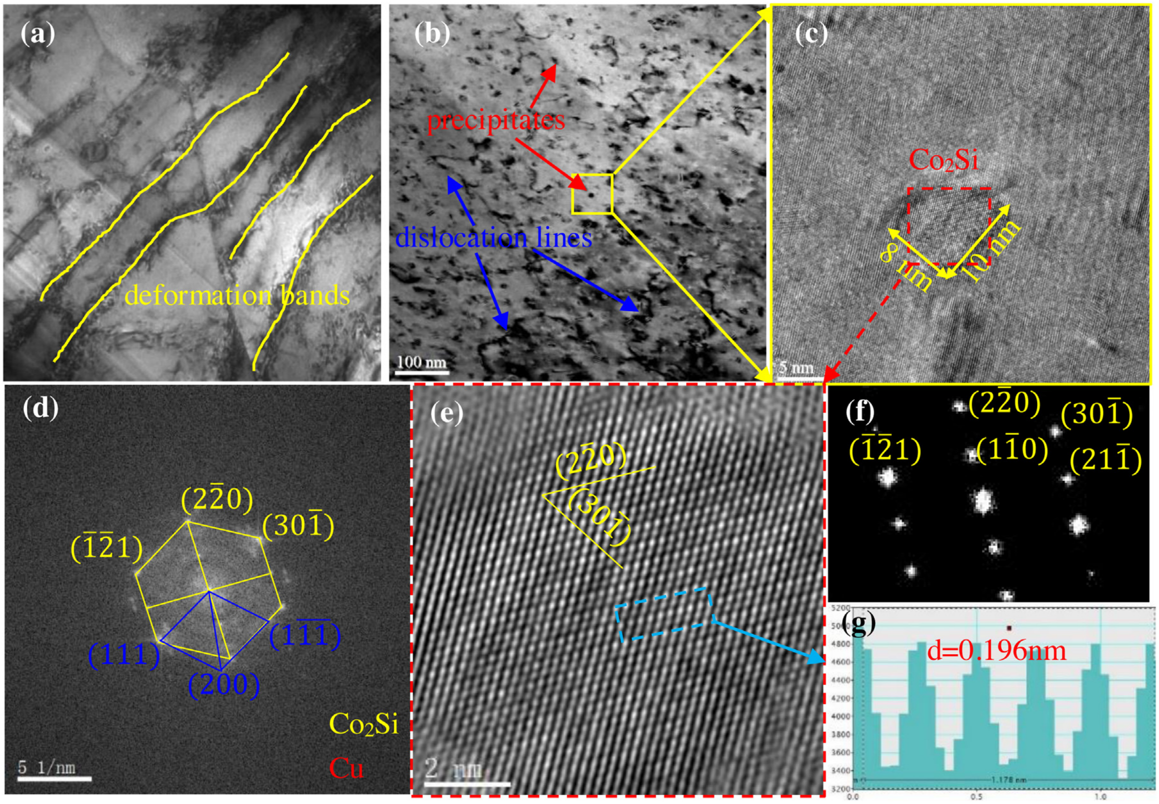

Fig. 8 – Microstructure of Cu-Co-Si-Ti alloy: (a), (b) TEM micrographs deformed at 700 °C and 0.01 s^{-1}; (c) HRTEM; (d) FFT of (c); (e), (f) IFFT of (h); (g) measurement of crystal surface spacing.

be concluded that the addition of Cr can make the precipitated phase finer and microstructure more homogeneous, and enhance the thermal deformation activation energy of the Cu-Ni-Si alloy after deformation. The constitutive equations of the two alloys are as follows:

For Cu-Ni-Co-Si alloy:

$$\dot{\varepsilon} = e^{63.38}[\sinh(0.009\sigma)]^{9.04}\exp(-\frac{569800}{8.314T})$$

For Cu-Ni-Co-Si-Cr alloy:

$$\dot{\varepsilon} = e^{75.35}[\sinh(0.005\sigma)]^{13.37}\exp(-\frac{639500}{8.314T})$$

Fig. 6 shows the electrical conductivity and ultimate tensile strength of Cu-Ni-Si alloy with the different trace alloy elements, such as Al, Mg, Co, Cr, Ti. It can be seen that the Cu-Ni-Si alloys have high strength but low conductivity due to the addition of Al and Mg. Lei et al. [86] found that the addition of aluminum promotes precipitation, effectively refines the grains and improves the stress relaxation resistance of the alloy. After 50% cold deformation and aging at 450 °C for 60 min, the peak properties of the Cu-Ni-Si-Al alloy were obtained: the conductivity was 28.1% IACS; the micro hardness was 343 HV; and the tensile strength was 1080 MPa. The Cu-Ni-Si alloy has high conductivity and low strength due to the addition of V or Zr. However, the addition of Ti, Co and P makes the Cu-Ni-Si alloy have high conductivity and strength at the same time, i.e. good comprehensive properties. Xiao et al. [96] got a high conductivity and strength of Cu-Ni-Si alloy by the Co addition. The results show that Co addition delayed the occurrence of Spinodal decomposition, which was explained by analyzing the microstructural observation. Zhang et al. [100] investigated the effects of P addition on microstructure and mechanical property of the Cu-Ni-Si-P alloy. After aging at 450 °C for 48 h, the semi coherent precipitates (δ-Ni_2Si) with the average size of 5 nm were observed in the microstructure by TEM analysis. At the same time, it also obtained the best comprehensive performance of 49% IACS and 804 MPa, which is attributed to the finer grains and acceleration of precipitation due to the addition of P. Ti element is more special, when the content is higher, the conductivity and strength of the alloy are relatively low. Liu et al. [104] investigated the aging strengthened Cu-3Ti-3Ni-0.5Si alloy with a high Ti content. Since the large solubility of Ti solute atoms in the Cu matrix enhances electron scattering, Cu-Ti alloys exhibit the poor electrical conductivity. Moreover, the precipitated phase particles transformed from Cu_4Ti phase to equilibrium and incoherent Cu_3Ti phase with aging, which greatly reduces the strength of Cu Ti alloy. However, when Ti content is low, it shows good comprehensive performance. Some researches [105–108] show that the addition of a small amount of Ti can refine grains and promote precipitation (δ-Ni_2Si), which can explain the reason of high conductivity and high strength for Cu-Ni-Si-Ti alloy. As for the addition of other alloy elements, there is no obvious characteristics.

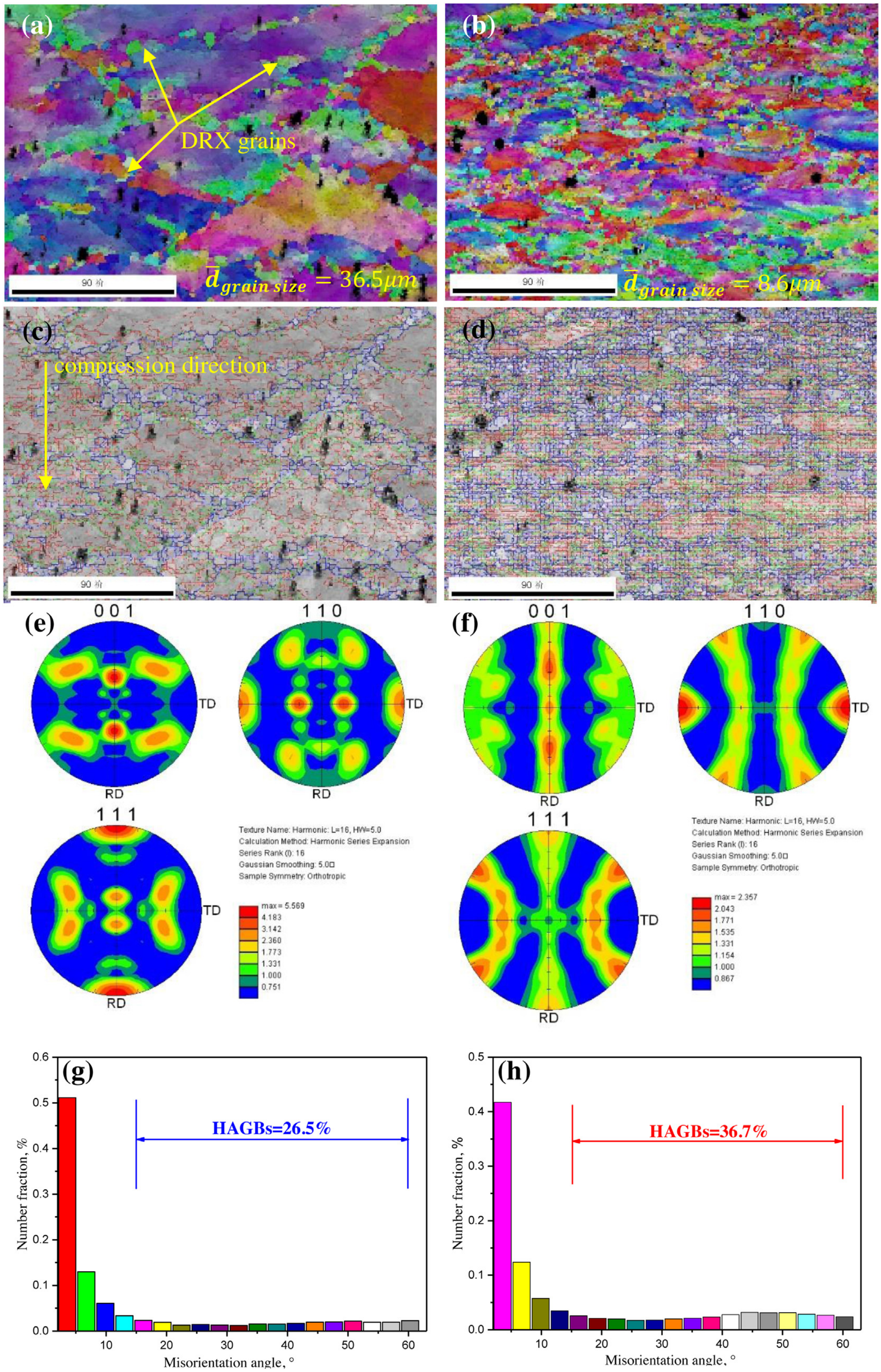

Fig. 9 – Microstructure of Cu-Fe-P alloy deformed at 0.01 s^{-1} with different temperature: (a) IPF map deformed at 700 °C; (b) IPF map deformed at 800 °C; (c) EBSD orientation maps of (a); (d) EBSD orientation maps of (b); (e) pole figures of (a); (f) pole figures of (b); (g) misorientation angle distribution of (a); (h) misorientation angle distribution of (b).

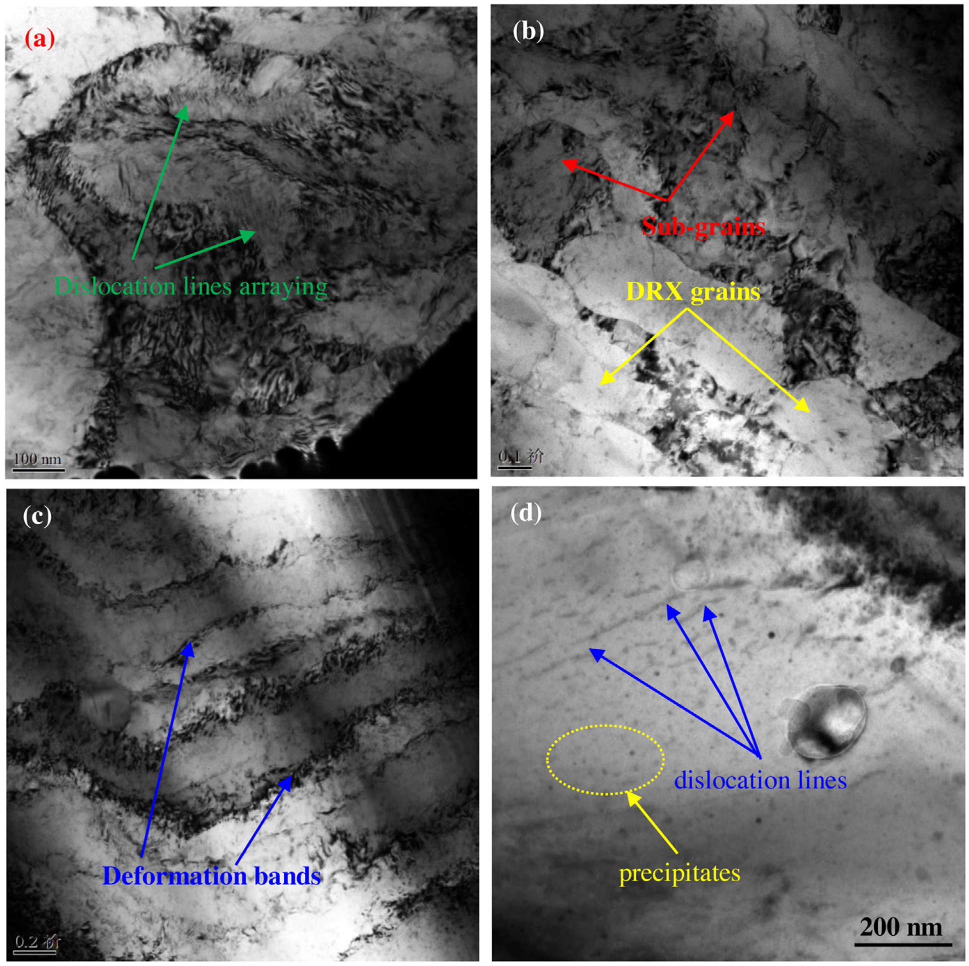

Fig. 10 – TEM micrographs of Cu-Fe-P alloy deformed at 700 °C, 0.01 s^{-1}.

3. Cu-Co-Si alloy

Liu et al. [109] investigated the texture distribution and precipitates of Cu-Ni-Si alloy at the aging process. With the increasing of aging temperature, the strength of copper texture {211} <111> and Goss texture {011} <100> decreased, while the strength of cubic texture {001} <100> increased, which can be attributed to the influence of precipitation (Ni_2Si) on the surrounding deformation area and then influence the texture strength. Lei et al. [110] obtained a high strength of Cu-Ni-Si alloy by analyzing the phase transformation and properties. The results shows that there are multi-precipitation phases (Ni_2Si, γ'-Ni_3Al, β-Ni_3Si), which play a significant role in improving the strength of studied alloy. Zhao et al. [16] and Xiao et al. [96] investigated the effects of Co addition on the electrical conductivity and mechanical properties of Cu-Ni-Si alloy. The electrical conductivity and mechanical properties are greatly improved due to the Orowan precipitation strengthening. In recent years, a lot of researches have been carried out based on the Cu-Ni-Si alloy by adding Co element, and the results show that the properties of the alloys are improved significantly by substituting a small amount of Co for Ni atom (δ-(Ni, Co)$_2$Si). Based on the above investigations, our team have a bold conjecture that the Co atom can completely replace the Ni atom and a small amount of Ti element is added, i.e. Cu-Co-Si-Ti alloy [29,111,112].

Fig. 7 shows the Kernel Average Misorientation (KAM) maps and corresponding ODF maps of Cu-Co-Si-Ti alloy deformed at 0.01 $s^{-1}$with different temperature of 700 °C and 800 °C. It is a kind of typical necklace structure, where a few fine recrystallized grains are around the deformed grains with an average grain size of 16.3 μm. Moreover, the HAGBs and LAGBs of the studied alloy deformed at 0.01 s^{-1} and 700 °C are 31.3% and 68.7%, respectively. With the deformed temperature increasing to 800 °C, the microstructure shows that the deformed grains are replaced by recrystallized grains and the microstructure becomes uniform. The average grain size is thus reduced to 14.3 μm. In addition, the content of HAGBs of the Cu-Co-Si-Ti alloy also increased, suggesting that the recrystallized volume fraction increases due to higher temperatures. As illustrated in Fig. 7(a), there are some unindexed regions in the Cu-Co-Si-Ti alloy under relatively low temperature deformation, which are similar to the Cu-Ni-Si alloy deformed at low temperature. Therefore, it can be inferred that there are more lattice distortion energy and dislocation

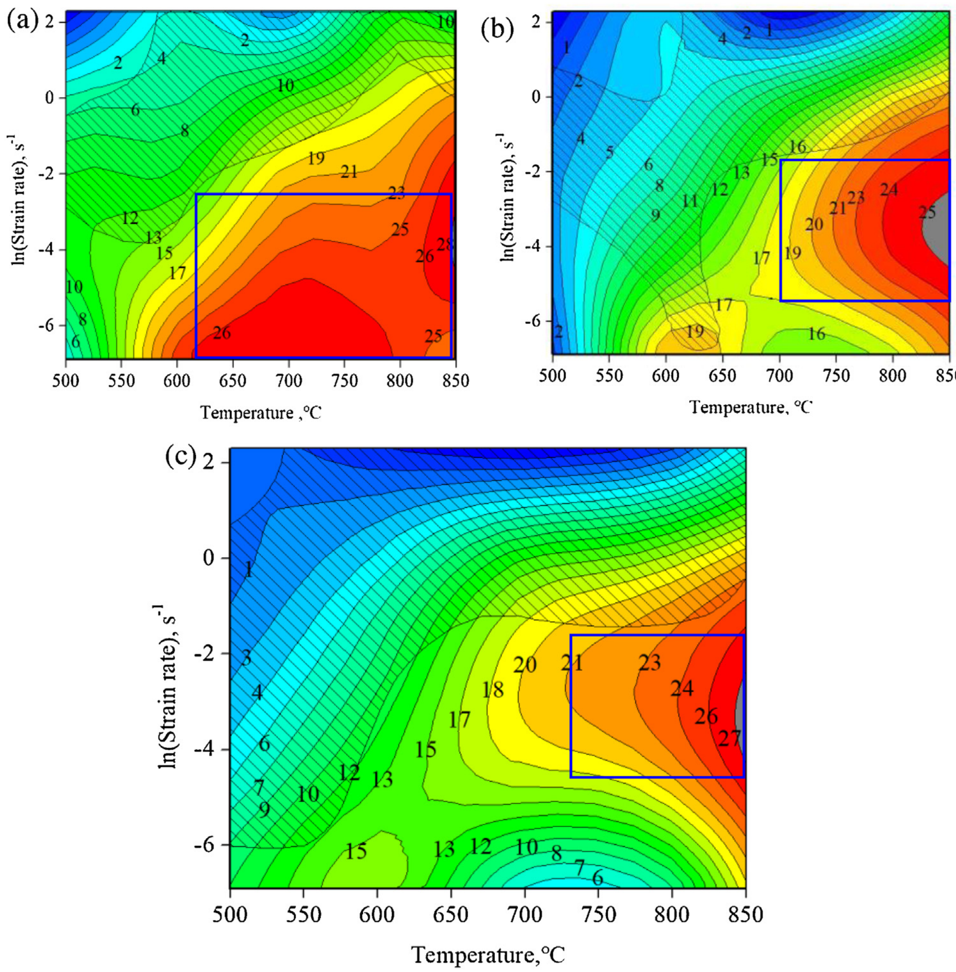

Fig. 11 – Hot processing maps of Cu-Fe-P (a), Cu-Fe-P-Ce (b) and Cu-Fe-P-Y (c) alloys.

energy around the deformed grains, which will be used for the nucleation of dynamic recrystallization grains [113,114]. As for the texture transformation of Cu-Co-Si-Ti alloy shown in the Fig. 7(c) and (d), it can be known that there are the {011} <100> Goss texture and {112} <111> copper texture deformed at 700 °C and 800 °C, respectively, by comparing the standard ODF maps in Fig. 2.

Fig. 8 shows the microstructure of Cu-Co-Si-Ti alloy deformed at 0.01 s^{-1} and 700 °C. As given in Fig. 8(a), there are some deformation bands in the microstructure, which can hinder the migration of grain boundaries and the movement of dislocations [115]. In addition, there are a lot of fine precipitates inside the grains, and some precipitates are surrounded by dislocation lines in Fig. 8(b). Fig. 8(c) shows the HRTEM image of the precipitates with the size of 8 nm × 10 nm in Fig. 8(b). It can be determined to be the Co_2Si with the lattice parameters of a = 7.109 nm, b = 4.918 nm and c = 3.737 nm by the diffraction pattern in Fig. 8(d). And the zone axis of Cu and Co_2Si is $[01\bar{1}]_{Cu}$ and $[113]_{Co2Si}$, respectively. Moreover, the directions of the $(2\bar{2}0)$ and $(30\bar{1})$ for the Co_2Si can be determined according to Fig. 8(d). Finally, the crystal surface spacing of the Co_2Si is 0.196 nm.

4. Cu-Fe-P alloy

Cu-Fe-P alloy is usually used as electronic components, such as semiconductor lead frame and electrical connector due to its high conductivity and medium strength [116,117]. The solubility of Fe in copper can reach 3.5% at 1050 °C while 0.15% at 635 °C. The addition of Fe has some benefits, such as refining the grains, delaying the recrystallization process and improving the mechanical properties of the copper alloy, although it will reduce the electrical conductivity and thermal conductivity of copper. The maximum solubility of P in copper matrix is 1.75%, which is almost 0% at the room temperature. In addition, P has a good effect on the mechanical properties and welding properties of copper alloys. Cao et al. [118] investigated the stability of the fine-grained microstructure of Cu-Fe-P alloy by the isothermal annealing. The results shows that the appearance of Fe_3P phase can refine the grains and improve the stability of microstructure, which was uniformly distributed in the grain interior and grain boundaries. Wang et al. [119] investigated the nanoscale precipitates evolution of Cu-Fe-P-Mg alloy by the aging treatment. And it can be inferred

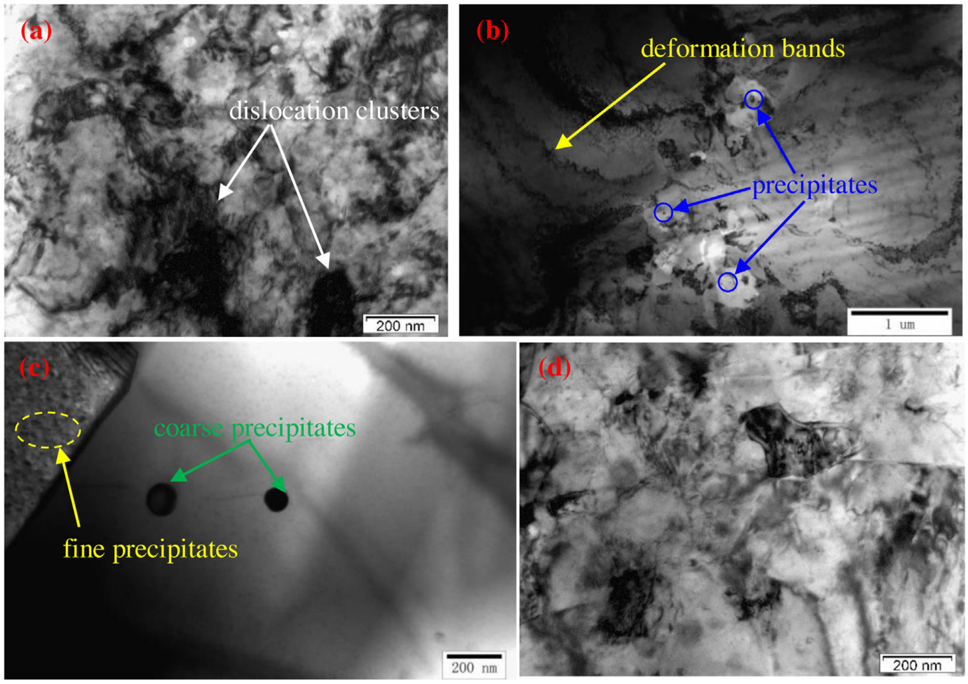

Fig. 12 – TEM micrographs of Cu-Fe-P alloy aging at 460 °C for 20 min.

that the precipitation of Mg_3P_2 phase inhibited the precipitation of Fe_3P particles, therefore, the alloy obtained an excellent comprehensive property of 599 MPa and 71.1%IACS.

Fig. 9 shows the microstructure evolution of Cu-Fe-P alloy deformed at 0.01 s^{-1} strain rate with different temperature. As shown in the Fig. 9(a) and (c), the recrystallized grains near the deformed grains have grown to an average size of 36.5 μm. With the temperature increasing to 800 °C, the recrystallized grains have grown at low temperature, and the deformed grains have recrystallized with average size of 8.6 μm. In addition, the texture of Cu-Fe-P alloy deformed at 700 °C and 800 °C can be determined as the {112} <111> copper texture and {111} <211> R texture, respectively, by the standard pole figures in Fig. 3, which is shown in the Fig. 9(e) and (f). Fig. 9(g) and (h) shows the misorientation angle distribution deformed at 700 °C and 800 °C, respectively. With the increasing of temperature, the percentage of high angle grain boundary increases. And it can be seen that the main distribution of the misorientation angle is concentrated at a small angle (LAGBs<15°), which is related to the stored dislocations [120]. The fraction of LAGBs in Fig. 9(g) and (h) can indicate that the dislocation density deformed at 700 °C is higher than that of deformed at 800 °C. Moreover, it can also inferred that the recrystallized volume fraction increases due to the increasing temperature. The TEM micrographs of Cu-Fe-P alloy deformed at 700 °C, 0.01 s^{-1} is shown in Fig. 10. As illustrated in Fig. 10(a), it can be seen that the dislocations rearrange near the grain boundaries in order to reduce the stress concentration under the early stage of deformation, which is an early character of dynamic recrystallization [112,121]. With the development of deformation, a small angle grain boundaries were formed in the deformed grains due to the cross-slip or climb of dislocations. Finally, the small angle grain boundaries were transformed into the recrystallized grains, which is characterized by almost no dislocation lines in the grains. In addition, there are some deformation bands and fine precipitated phase particles in the microstructure, which can hinder the migration of grain boundaries and movement of dislocations. The precipitates can be determined to be CuP_2 [46].

In the process of hot working, the deformation temperature and strain rate have great influence on the properties of the material after deformation. In order to reduce the deformation and cracking of materials, reduce the waste of resources and obtain the best hot working performance, the hot working diagram is drawn based on the Dynamic Material Modeling (DMM), which can determine the hot working process parameters (including deformation temperature and strain rate) [122–124]. The best hot working area can be found directly from the hot working diagram, and the working area that should be avoided in the process of alloy hot deformation can also be determined. Wu et al. [125] obtained the parameters suitable for hot working based on the processing maps with 1100–1200 °C /0.01–0.5 s^{-1} and 1100–1200 °C /1.0-10 s^{-1}. Fig. 11 shows the hot processing maps of Cu-Fe-P, Cu-Fe-P-Ce and Cu-Fe-P-Y alloys. The grid area in the figure is unstable, while other areas are stable. Moreover, the number on the lines indicates the power dissipation value, and the size of the value indicates the amount of energy consumed by microstructure evolution. Therefore, the suitable hot working areas of the three alloys are 620–850 °C, 0.001–0.08 s^{-1}; 700–850 °C, 0.001–0.14 s^{-1} and 720–850 °C, 0.001–0.16 s^{-1}, respectively.

Besides the thermal deformation behavior of copper alloys, it is also critical to investigate the aging behavior of copper alloy. Fig. 12 shows the TEM micrographs of Cu-Fe-P alloy aging at 460 °C for 20 min. It can be seen that there are some defor-

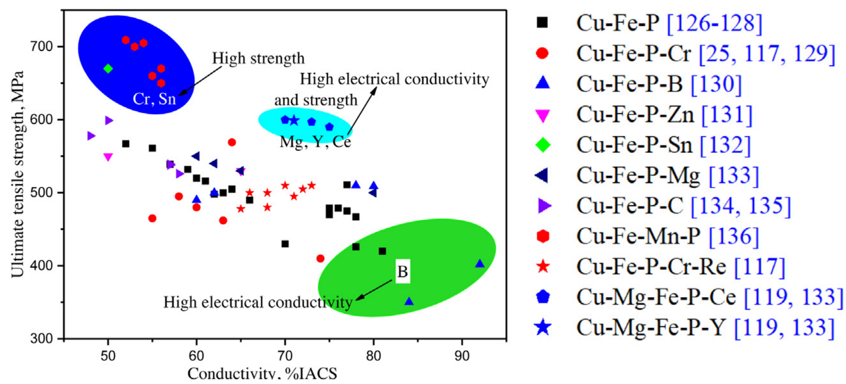

Fig. 13 – The comprehensive properties of the Cu-Fe-P alloy with different types of alloy elements[25,117,119,126–136].

mation bands, sub-grains and dislocated cells agglomerated together, which can hinder the migration of grain boundaries. In addition, there are fine precipitated phase particles with dispersion distribution and a small amount of growing precipitation phase, which can be determined to be α-Fe [119]. In order to study the effect of adding elements on the conductivity and tensile strength of the Cu-Fe-P alloy, Fig. 13 show the relationship between electrical conductivity and ultimate tensile strength of the Cu-Fe-P alloys with different types of alloy elements. It can be seen that the addition of Cr and Sn makes the strength of the Cu-Fe-P alloy higher and the conductivity more decreased. Guo et al. [117] investigated the conductivity and mechanical properties of Cu-Fe-P alloy, the results show that the addition of Cr can significantly improve the physical properties and mechanical properties by promoting the dispersion of precipitated phase in matrix. Lu et al. [130] obtained a high electrical conductivity of Cu-Fe-P alloy by the B addition, which has a little negative effect on conductivity, but the tensile strength was relatively low. It is worth mentioning that the addition of Mg, Y and Ce elements has a good comprehensive performance for Cu-Fe-P alloy. Wang et al. [119] obtained a high conductivity and mechanical properties of Cu-Fe-P alloy by the addition of Y with a combined performance of 599 MPa and 71.1%IACS, which was attributed to the aging precipitation strengthening. In the end, other added elements have no significant effect on the Cu-Fe-P alloy for conductivity and mechanical properties.

5. Conclusions

In this review, the texture evolution and microstructure evolution under hot deformation of Cu-Ni-Si, Cu-Co-Si and Cu-Fe-P alloys were investigated. In order to analyze the texture evolution, the standard polar figures and ODF figures were established. The TEM analysis shows that the addition of trace elements promoted the dispersion of nanoscale precipitated phase particles in the matrix, which can hinder the movement of grain boundaries and dislocations during the hot deformation or aging processes. In addition, the suitable hot processing parameters of the Cu-Fe-P alloy were determined by the hot working diagram. Finally, the comprehensive diagrams for the influence of the alloying elements addition on the electrical conductivity and ultimate tensile strength of the Cu-Ni-Si and Cu-Fe-P alloys were obtained.

Conflicts of interest

The authors declare no conflicts of interest.

Author Biography

Yongfeng Geng, Yijie Ban, Yi Zhang, Yanlin Jia, Baohong Tian, Yong Liu, Alex A. Volinsky, Kexing Song are mainly engaged in the research of thermal deformation and aging of advanced copper alloys; Bingjie, Wang is mainly engaged in the research of high entropy alloy; Xu Li is mainly engaged in the research of electron microscopy and stress measurement technology.

So far, three papers have been published in JAC and Vacuum as the first author (Yongfeng Geng, DOI: https://doi.org/10.1016/j.jallcom.2019.153518; https://doi.org/10.1016/j.vacuum.2020.109376;https://doi.org/10.1016/j.jallcom.2020.155666). In these three papers, the hot deformation behavior of Cu-Co-Si alloy and the effect of Ti and Ce addition on the hot deformation behavior of the alloy were investigated, mainly including the stress-strain curve, EBSD analysis and TEM characterization. The results show that the addition of alloying elements can inhibit the recrystallization of the alloy and improve the activation energy of hot deformation, which has a good effect.

Acknowledgments

This work was supported by the Open Cooperation Project of Science and Technology of the Henan Province (182106000018), Henan University Scientific and Technological Innovation Talent Support Program (18HASTIT024) and the National Natural Science Foundation of China (U1704143).

REFERENCES

[1] Shukla AK, Narayana Murty SVS, Sharma SC, Mondal K. Constitutive modeling of hot deformation behavior of

vacuum hot pressed Cu-8Cr-4Nb alloy. Mater Des 2015;75:57–64.
[2] Liu KM, Lu DP, Zhou HT, Chen ZB, Atrens A, Lu L. Influence of a high magnetic field on the microstructure and properties of a Cu-Fe-Ag in situ composite. Mater. Sci. Eng. A 2013;584:114–20.
[3] Tian YZ, Freudenberger J, Pippan R, Zhang ZF. Formation of nanostructure and abnormal annealing behavior of a Cu-Ag-Zr alloy processed by high-pressure torsion. Mater. Sci. Eng. A 2013;568:184–94.
[4] Liu KM, Jiang ZY, Zhao JW, Zou J, Chen ZB, Lu DP. Effect of directional solidification rate on the microstructure and properties of deformation-processed Cu-7Cr-0.1Ag in situ composites. J Alloys Compd 2014;612:221–6.
[5] Zhang Y, Sun HL, Volinsky Alex A, Tian BH, Song KX, Wang BJ, et al. Hot workability and constitutive model of the Cu-Zr-Nd alloy. Vacuum 2017;146:35–43.
[6] Guo XL, Xiao Z, Qiu WT, Li Z, Zhao ZQ, Wang X, et al. Microstructure and properties of Cu-Cr-Nb alloy with high strength, high electrical conductivity and good softening resistance performance at elevated temperature. Mater. Sci. Eng. A 2019;749:281–90.
[7] Liu KM, Jiang ZY, Zhou HT, Lu DP, Atrens A, Yang YL. Effect of heat treatment on the microstructure and properties of deformation-processed Cu-7Cr in situ composites. J Mater Eng Perform 2015;24(11):4340–5.
[8] Luo BM, Li DX, Zhao C, Wang Z, Luo ZQ, Zhang WW. A low Sn content Cu-Ni-Sn alloy with high strength and good ductility. Mater. Sci. Eng. A 2019;746:154–61.
[9] Xu S, Fu Hd, Wang YT, Xie JX. Effect of Ag addition on the microstructure and mechanical properties of Cu-Cr alloy. Mater. Sci. Eng. A 2018;726:208–14.
[10] Sun XL, Jie JC, Wang PF, Qin BL, Ma XD, Wang TM, et al. Effects of Co and Si additions and cryogenic rolling on structure and properties of Cu-Cr alloys. Mater. Sci. Eng. A 2019;740-741:165–73.
[11] Wang ZQ, Zhong YB, Cao GH, Wang C. Influence of dc electric current on the hardness of thermally aged Cu-Cr-Zr alloy. J Alloys Compd 2009;479:303–6.
[12] Liu KM, Jiang ZY, Zhao JW, Zou J, Lu L, Lu DP. Thermal stability and properties of deformation-processed Cu-Fe in situ composites. Metal. Mater. Trans. A 2015;46(5):2255–61.
[13] Hu T, Chen JH, Liu JZ, Liu ZR, Wu CL. The crystallographic and morphological evolution of the strengthening precipitates in Cu-Ni-Si alloys. Acta Mater 2013;61(4):1210–9.
[14] Zhang XH, Zhang Y, Tian BH, Song KX, Liu P, Jia YL, et al. Review of nano-phase effects in high strength and conductivity copper alloys. Nanotechnol Rev 2019;8:383–95.
[15] Guo CJ, Chen JS, Xiao XP, Huang H, Wang WJ, Yang B. The effect of Co addition on the modulated structure coarsening and discontinuous precipitation growth kinetics of Cu-15Ni-8Sn alloy. J Alloys Compd 2020;835:155275.
[16] Zhao Z, Zhang Y, Tian BH, Jia YL, Liu Y, Song KX, et al. Co effects on Cu-Ni-Si alloys microstructure and physical properties, J. Alloy. Compd 2019;797:1327–37.
[17] Ren CX, Wang Q, Hou JP, Zhang ZJ, Yang HJ, Zhang ZF. Exploring the strength and ductility improvement of Cu-Al alloys. Mater. Sci. Eng. A 2020;786:139441.
[18] Zhang YF, Yuan XG, Huang HJ, Zuo XJ, Cheng YL. Influence of chloride ion concentration and temperature on the corrosion of Cu-Al composite plates in salt fog. J Alloys Compd 2020;821:153249.
[19] Velazquez D, Chaparro MAE, Bohnel HN, Romero R, Lanzini F. Spinodal decomposition, chemical and magnetic ordering in Cu-Al-Mn shape memory alloys. Mater Chem Phys 2020;246:122793.
[20] Sun YQ, Peng LJ, Huang GJ, Xie HF, Mi XJ, Liu XH. Effects of Mg addition on the microstructure and softening resistance of Cu-Cr alloys. Mater. Sci. Eng. A 2020;776:139009.
[21] Ma MZ, Li Z, Qiu WT, Xiao Z, Zhao ZL, Jiang YB, et al. Development of homogeneity in a Cu-Mg-Ca alloy processed by equal channel angular pressing. J Alloys Compd 2020;820:153112.
[22] Gholami M, Altenberger I, Vesely J, Kuhn H-A, Wollmann M, Janecek M, et al. Effects of severe plastic deformation on transformation kinetics of precipitates in CuNi3Si1Mg. Mater. Sci. Eng. A 2016;676:156–64.
[23] Zou J, Lu DP, Fu QF, Liu KM, Jiang J. Microstructure and properties of Cu-Fe deformation processed in-situ composite. Vacuum 2019;167:54–8.
[24] Sun XJ, He J, Chen B, Zhang LL, Jiang HX, Zhao JZ, et al. Microstructure formation and electrical resistivity behavior of rapidly solidified Cu-Fe-Zr immiscible alloys. J Mater Sci Technol Res 2020;44:201–8.
[25] Liu KM, Huang ZK, Zhang XW, Lu DP, Atrens A, Zhou HT, et al. Influence of Ag micro-alloying on the thermal stability and ageing characteristics of a Cu-14Fe in-situ composite. Mater. Sci. Eng. A 2016;673:1–7.
[26] Zhao C, Wang Z, Li DX, Pan DQ, Lou BM, Luo ZQ, et al. Optimization of strength and ductility in an as-extruded Cu-15Ni-8Sn alloy by the additions of Si and Ti. J Alloys Compd 2020;823:153759.
[27] Yuan JH, Gong LK, Zhang WQ, Zhang B, Wei HG, Xiao XP, et al. Work softening behavior of Cu-Cr-Ti-Si alloy during cold deformation. J. Mater. Res. Technol 2019;8(2):1964–70.
[28] Zhao B, T.Y. Y, Ding WF, Zhang LC, Su HH, Chen ZZ. Effect of micropores on the microstructure and mechanical properties of porous Cu-Sn-Ti composites. Mater. Sci. Eng. A 2018;730:345–54.
[29] Geng YF, Li X, Zhou HL, Zhang Y, Jia YL, Tian BH, et al. Effect of Ti addition on microstructure evolution and precipitation in Cu-Co-Si alloy during hot deformation. J Alloys Compd 2020;821:153518.
[30] Liu Y, Shao S, Liu KM, Yang XJ, Lu DP. Microstructure refinement mechanism of Cu-7Cr in situ composites with trace Ag. Mater. Sci. Eng. A 2012;531:141–6.
[31] Liu KM, Wang ZX, Jiang ZY, Atrens A, Huang ZK, Guo W, et al. Cu-7Cr-0.1Ag microcomposites optimized for high strength and high conductivity. J Mater Eng Perform 2018;27(3):933–8.
[32] Sun HL, Zhang Y, Volinsky AA, Wang BJ, Tian BH, Song KX, et al. Effects of Ag addition on hot deformation behavior of Cu-Ni-Si Alloys, A. Eng. Mater 2017;19:1600607.
[33] Zhao ZQ, Xiao Z, Li Z, Ma MZ, Dai J. Effect of magnesium on microstructure and properties of Cu-Cr alloy. J Alloys Compd 2018;752:191–7.
[34] Sarkara A, Prasada MJNV, Narayana Murty SVS. Effect of initial grain size on hot deformation behavior of Cu-Cr-Zr-Ti alloy. J Miner Mater Charact Eng 2020;160:110112.
[35] Ban YJ, Zhang Y, Jia YL, Tian BH, Volinsky Alex A, Zhang XH, et al. Effects of Cr addition on the constitutive equation and precipitated phases of copper alloy during hot deformation. Mater Des 2020;191:108613.
[36] Wang JF, Chen JS, Guo CJ, Zhang JB, Xiao XP, Yang B. Effect of heat treatment on low cycle fatigue properties of Cu-Cr-Zr alloy. J Miner Mater Charact Eng 2019;158:109940.
[37] Fu HD, Xu S, Li W, Xie JX, Zhao HB, Pan ZJ. Effect of rolling and aging processes on microstructure and properties of Cu-Cr-Zr alloy. Mater. Sci. Eng. A 2017;700:107–15.
[38] Tian W, Bi LM, Ma FC, Du JD. Effect of Zr on as-cast microstructure and properties of Cu-Cr alloy. Vacuum 2018;149:238–47.
[39] Kim H, Ahn JH, Han SZ, Jo J, Baik H, Kim M, et al. Microstructural characterization of cold-drawn Cu-Ni-Si

alloy having high strength and high conductivity. J Alloys Compd 2020;832:155059.
[40] Geng GH, Wang DX, Zhang WR, Liu LM, Laptev AM. Fabrication of Cu-Ni-Si alloy by melt spinning and its mechanical and electrical properties. Mater. Sci. Eng. A 2020;776:138979.
[41] Diánez MJ, Donoso E, Criado JM, Sayagués MJ, Díaz G, Olivares L. Study by DSC and HRTEM of the aging strengthening of Cu-Ni-Zn-Al alloys. Mater Des 2016;92:184–8.
[42] Pereira EC, Matlakhova LA, Matlakhov AN, de Araújo CJ, Shigue CY, Monteiro SN. Reversible martensite transformations in thermal cycled polycrystalline Cu-13.7%Al-4.0%Ni alloy. J Alloys Compd 2016;688:436–46.
[43] Mishnev R, Shakhova I, Belyakov A, Kaibyshev R. Deformation microstructures, strengthening mechanisms, and electrical conductivity in a Cu-Cr-Zr alloy. Mater. Sci. Eng. A 2015;629:29–40.
[44] Zhou JM, Zhu DG, Tang LT, Jiang XS, Chen S, Peng X, et al. Microstructure and properties of powder metallurgy Cu-1%Cr-0.65%Zr alloy prepared by hot pressing. Vacuum 2016;131:156–63.
[45] Ji GL, Li Q, Li L. A physical-based constitutive relation to predict flow stress for Cu-0.4Mg alloy during hot working. Mater. Sci. Eng. A 2014;615:247–54.
[46] Wang BJ, Zhang Y, Tian BH, Yakubov V, An JC, Volinsky Alex A, et al. Effects of Ce and Y addition on microstructure evolution and precipitation of Cu-Mg alloy hot deformation. J Alloys Compd 2019;781:118–30.
[47] Lei Q, Li Z, Gao Y, Peng X, Derby B. Microstructure and mechanical properties of a high strength Cu-Ni-Si alloy treated by combined aging processes. J Alloys Compd 2017;695:2413–23.
[48] Chalon J, Guérin JD, Dubar L, Dubois A, Puchi-Cabrera ES. Characterization of the hot-working behavior of a Cu-Ni-Si alloy. Mater. Sci. Eng. A 2016;667:77–86.
[49] Fu HD, Xu S, Li W, Xie JX, Zhao HB, Pan ZJ. Effect of rolling and aging processes on microstructure and properties of Cu-Cr-Zr alloy. Mater. Sci. Eng. A 2017;700:107–15.
[50] Shen DP, Zhou HB, Tong WP. Grain refinement and enhanced precipitation of Cu-Cr-Zr induced by hot rolling with intermediate annealing treatment. J. Mater. Res. Technol 2019;8(5):5041–5.
[51] Wang BJ, Zhang Y, Tian BH, An JC, Volinsky Alex A, Sun HL, et al. Effects of Ce addition on the Cu-Mg-Fe alloy hot deformation behavior. Vacuum 2018;155:594–603.
[52] Zhang Y, Volinsky Alex A, Tran HT, Chai Z, Liu P, Tian BH, et al. Aging behavior and precipitates analysis of the Cu-Cr-Zr-Ce alloy. Mater. Sci. Eng. A 2016;650:248–53.
[53] Gao LQ, Yang X, Zhang XF, Zhang Y, Sun HL, Li N. Aging behavior and phase transformation of the Cu-0.2 wt%Zr-0.15 wt %Y alloy. Vacuum 2019;159:367–73.
[54] Zhang Y, Chai Z, Volinsky Alex A, Tian BH, Sun HL, Liu P, et al. Processing maps for the Cu-Cr-Zr-Y alloy hot deformation behavior. Mater. Sci. Eng. A 2016;662:320–9.
[55] Bhattacharjee PP, Tsuji N, Ray RK. Effect of initial grain size on the evolution of {001}<100> texture in severely deformed and annealed high purity Nickel. Metall. Mater. Trans. A 2011;42:2769–80.
[56] Lei Q, Li Z, Hu WP, Liu Y, Meng CL, Derby B, et al. Microstructure evolution and hardness of an ultra-high strength Cu-Ni-Si alloy during thermo-mechanical processing. J Mater Eng Perform 2016;25:2615–25.
[57] Haase C, Barrales-Mora LA. Influence of deformation and annealing twinning on the microstructure and texture evolution of face-centered cubic high-entropy alloys. Acta Mater 2018;150:88–103.
[58] P.Bhattacharjee P, Joshi M, Chaudhary VP, Gatti JR, Zaid M. Texture evolution during cross rolling and annealing of high purity nickel. Metall. Mater. Trans. A 2013;44:2707–16.
[59] Reddy SR, Ahmed MZ, Sathiaraj GD, Bhattacharjee PP. Effect of strain path on microstructure and texture formation in cold-rolled and annealed FCC equiatomic CoCrFeMnNi high entropy alloy. Inter 2017;87:94–103.
[60] Bhattacharjee PP, Joshi M, Chaudhary VP, Zaid M. The effect of starting grain size on the evolution of microstructure and texture in nickel during processing by cross-rolling. J Miner Mater Charact Eng 2013;76:21–7.
[61] Bhattacharjee PP, Saha S, Gatti JR. Effect of change in strain path during cold rolling on the evolution of microstructure and texture in Al and Al-2.5%Mg. J Mater Eng Perform 2014;23:458–68.
[62] Suwas S, Singh AK. Role of strain path change in texture development. Mater. Sci. Eng. A 2003;356(1-2):368–71.
[63] Gurao NP, Sethuraman S, Suwas S. Effect of strain path change on the evolution of texture and microstructure during rolling of copper and nickel. Mater. Sci. Eng. A 2011;528(25-26):7739–50.
[64] Mondal C, Singh AK, Mukhopadhyay AK, Chattopadhyay K. Tensile flow and work hardening behavior of hot cross-rolled AA7010 aluminium alloy sheets. Mater. Sci. Eng. A 2013;577:87–100.
[65] Bhattacharjee PP, Ray RK, Tsuji N. Cold-rolling and recrystallization textures of a Ni-5at.%W alloy. Acta Mater 2009;57:2166–79.
[66] Yang X, Zhang JX, Gong YL, Nakatani M, Sharma B, Ameyama K, et al. A superior strength-ductility combination in gradient structured Cu-Al-Zn alloys with proper stacking fault energy and processing time. Mater. Sci. Eng. A 2020;789:139619.
[67] Ray RK, Bhattacharjee PP. Enhancement of cube texture in Ni by the addition of W or Mo. Philos Mag 2007;87:2417–26.
[68] Yi J, Jia YL, Zhao YY, Xiao Z, He KJ, Wang Q, et al. Precipitation behavior of Cu-3.0Ni-0.72Si alloy. Acta Mater 2019;166:261–70.
[69] Tsubakino H, Nozato R, Yamamoto A. Precipitation sequence for simultaneous continuous and discontinuous modes in Cu-Be binary alloys. Mater Sci Technol 1993;9(4):288–94.
[70] Sierpinski Z, Gryziecki J. Phase transformations and strengthening during aging of CuNi10Al3 alloy. Mater. Sci. Eng. A 1999;264:279–85.
[71] Jeon WS, Shur CC, Kim JG, Han SZ, Kim YS. Effect of Cr on the corrosion resistance of Cu-6Ni-4Sn alloys. J Alloys Compd 2008;455:358–63.
[72] Lei Q, Li Z, Zhu A, Qiu W, Liang S. The transformation behavior of Cu-8.0Ni-1.8Si-0.6Sn-0.15Mg alloy during isothermal heat treatment. J Miner Mater Charact Eng 2011;62(9):904–11.
[73] Lei Q, Li Z, Wang MP, Zhang L, Gong S, Xiao Z, et al. Phase transformations behavior in a Cu-8.0Ni-1.8Si alloy. J Alloys Compd 2011;509:3617–22.
[74] Li Z, Pan ZY, Zhao YY, Xiao Z, Wang MP. Microstructure and properties of high conductivity, super high strength Cu-8.0Ni-1.8Si-0.6Sn-0.15Mg alloy. J Mater Res 2009;24:2123–9.
[75] Pan ZY, Wang MP, Li Z, Deng CP, Li SH, Jia YL. Progress of study of super-high strength Cu-Ni-Si alloy. Heat. Treat. Met 2007;7:55–9.
[76] Xie H, Jia L, Lu ZL. Microstructure and solidification behavior of Cu-Ni-Si alloys. J Miner Mater Charact Eng 2009;60:114–8.
[77] Lee S, Matsunaga H, Sauvage X, Horita Z. Strengthening of Cu-Ni-Si alloy using high-pressure torsion and aging. Mater Charact 2014;90:62–70.

[78] Suzuki S, Shibutani N, Mimura K, Isshiki M, Waseda Y. Improvement in strength and electrical conductivity of Cu-Ni-Si alloys by ageing and cold rolling. J Alloys Compd 2006;417:116–20.
[79] Zhao DM, Dong QM, Liu P, Kang BX, Huang JL, Jin ZH. Structure and strength of the age hardened Cu-Ni-Si alloy. Mater Chem Phys 2003;79:81–6.
[80] Kim YG, Seong TY, Han JH. Effect of heat treatment on precipitation behavior in a Cu-Ni-Si-P alloy. J Mater Sci 1986;21:1357–62.
[81] Watanabe C, Hiraide H, Zhang ZG, Monzen R. Microstructure and mechanical properties of Cu-Ni-Si alloys. J. Soc. Sci. Jpn 2005;54:717–23.
[82] Guan DK, Rainforth WM, Gao JH, Sharp J, Wynne B, Ma L. Individual effect of recrystallisation nucleation sites on texture weakening in a magnesium alloy: part 1- double twins. Acta Mater 2017;135:14–24.
[83] Heidarzadeh A, Saeid T, Klemmc V, Chabok A, Pei YT. Effect of stacking fault energy on the restoration mechanisms and mechanical properties of friction stir welded copper alloys. Mater Des 2019;162:185–97.
[84] Liu SH, Pan QL, Li MJ, Wang XD, He X, Li XY, et al. Microstructure evolution and physical-based diffusion constitutive analysis of Al-Mg-Si alloy during hot deformation. Mater Des 2019;184:108181.
[85] Jia D, Sun WR, Xu DS, Liu F. Dynamic recrystallization behavior of GH4169G alloy during hot compressive deformation. J Mater Sci Technol 2019;35:1851–9.
[86] Lei Q, Li Z, Dai C, Wang J, Chen X, Xie JM, et al. Effect of aluminum on microstructure and property of Cu-Ni-Si alloys. Mater. Sci. Eng. A 2013;572:65–74.
[87] Lei Q, Li SY, Zhu JL, Xiao Z, Zhang FF, Li Z. Microstructural evolution, phase transition, and physics properties of a high strength Cu-Ni-Si-Al alloy. J Miner Mater Charact Eng 2019;147:315–23.
[88] Wang W, Kang HJ, Chen ZQ, Chen ZJ, Zou CL, Li RG, et al. Effects of Cr and Zr additions on microstructure and properties of Cu-Ni-Si alloys. Mater. Sci. Eng. A 2016;673:378–90.
[89] Wu YK, Li Y, Lu JY, Tan S, Jiang F, Sun J. Correlations between microstructures and properties of Cu-Ni-Si-Cr alloy. Mater. Sci. Eng. A 2018;731:403–12.
[90] Wu YK, Li Y, Lu JY, Tan S, Jiang F, Sun J. Effects of pre-deformation on precipitation behaviors and properties in Cu-Ni-Si-Cr alloy. Mater. Sci. Eng. A 2019;742:501–7.
[91] Cheng JY, Tang BB, Yu FX, Shen B. Evaluation of nanoscale precipitates in a Cu-Ni-Si-Cr alloy during aging. J Alloys Compd 2014;614:189–95.
[92] Xiao XP, Xiong BQ, Wang QS, Xie GL, Peng LJ, Huang GX. Microstructure and properties of Cu-Ni-Si-Zr alloy after thermomechanical treatments. Rare Met Mater Eng 2013;32(2):144–9.
[93] Huang JZ, Xiao Z, Dai J, Li Z, Jiang HY, Wang W, et al. Microstructure and properties of a novel Cu-Ni-Co-Si-Mg alloy with super-high strength and conductivity. Mater. Sci. Engi. A 2019;744:754–63.
[94] Zhao ZL, Xiao Z, Li Z, Qiu WT, Jiang HY, Lei Q, et al. Microstructure and properties of a Cu-Ni-Si-Co-Cr alloy with high strength and high conductivity. Mater. Sci. Eng. A 2019;759:396–403.
[95] Li J, Huang GJ, Mi XJ, Peng LJ, Xie HF, Kang YL. Microstructure evolution and properties of a quaternary Cu-Ni-Co-Si alloy with high strength and conductivity. Mater. Sci. Eng. A 2019;766:138390.
[96] Xiao XP, Yi ZY, Chen TT, Liu RQ, Wang H. Suppressing spinodal decomposition by adding Co into Cu-Ni-Si alloy. J Alloys Compd 2016;660:178–83.
[97] Chen W, Wang MP, Li Z, Dong QY, Jia YL, Xiao Z, et al. A novel Cu-10Zn-1.5Ni-0.34Si alloy with excellent mechanical property through precipitation hardening. J Mater Eng Perform 2016;25:4624–30.
[98] Krishna SC, Srinath J, Jha AK, Pant B, Sharma SC, George KM. Microstructure and properties of a high-strength Cu-Ni-Si-Co-Zr alloy. J Mater Eng Perform 2013;22:2115–20.
[99] Han SZ, Gu JH, Lee JH, Que ZP, Shin JH, Lim SH, et al. Effect of V addition on hardness and electrical conductivity in Cu-Ni-Si alloys. Met. Mater. Int 2013;19:637–41.
[100] Zhang Y, Tian BH, Volinsky Alex A, Sun HL, Chai Z, Liu P, et al. Microstructure and precipitate's characterization of the Cu-Ni-Si-P alloy. J Mater Eng Perform 2016;25:1336–41.
[101] Zhao DM, Dong QM, Liu P, Kang BX, Huang JL, Jin ZH. Structure and strength of the age hardened Cu-Ni-Si alloy. Mater Chem Phys 2003;79:81–6.
[102] Han SZ, Lee J, Lim SH, Ahn JH, Kim K, Kim S. Optimization of conductivity and strength in Cu-Ni-Si alloys by suppressing discontinuous precipitation. Met. Mater. Int 2016;22:1049–54.
[103] Stavroulakis P, Toulfatzis A, Vazdirvanidis A, Pantazopoulos G, Papaefthymiou S. Investigation of the aging behavior of a Cu-Ni-Si rolled alloy. Metall. Micro. Anal 2019;8:167–81.
[104] Liu J, Wang XH, Chen J, Liu JT. The effect of cold rolling on age hardening of Cu-3Ti-3Ni-0.5Si alloy. J Alloys Compd 2019;797:370–9.
[105] Kim HG, Lee TW, Kim SM, Han SZ, Euh K, Kim WY, et al. Effects of Ti addition and heat treatments on mechanical and electrical properties of Cu-Ni-Si alloys. Met. Mater. Int 2013;19:61–5.
[106] Lee E, Han S, Euh K, Lim S, Kim S. Effect of Ti addition on tensile properties of Cu-Ni-Si alloys. Met. Mater. Int 2011;17:569–76.
[107] Lee E, Euh K, Han SZ, Lim S, Lee J, Kim S. Tensile and electrical properties of direct aged Cu-Ni-Si-x%Ti alloys. Met. Mater. Int 2013;19:183–8.
[108] Watanabe C, Takeshita S, Monzen R. Effects of small addition of Ti on strength and microstructure of a Cu-Ni-Si alloy. Metall. Mater. Trans. A 2015;46:2469–75.
[109] Liu ZS, Chen YL, Wei H, Li ZC. Study on the distribution of texture and the second phase under different aging process of Cu-Ni-Si alloy. Mater. Letters 2019;236:292–4.
[110] Lei Q, Xiao Z, Hu WP, Derby B, Li Z. Phase transformation behaviors and properties of a high strength Cu-Ni-Si alloy. Mater. Sci. Eng. A 2017;697:37–47.
[111] Geng YF, Li X, Zhang Y, Jia YL, Zhou HL, Tian BH, et al. X.H. Chen. Vacuum 2020;177:109376.
[112] Geng YF, Zhang Y, Song KX, Jia YL, Li X, Stock H, et al. X.H. Chen. J Alloys Compd 2020;842:155666.
[113] Zhao QY, Yang F, Torrens R, Bolzoni L. Comparison of hot deformation behavior and microstructural evolution for Ti-5Al-5V-5Mo-3Cr alloys prepared by powder metallurgy and ingot metallurgy approaches. Mater Des 2019;169:107682.
[114] Wu YS, Qin XZ, Wang CS, Zhou LZ. Influence of phosphorus on hot deformation microstructure of a Ni-Fe-Cr based alloy. Mater. Sci. Eng. A 2019;768:138454.
[115] Zhong XT, Wang L, Huang LK, Liu F. Transition of dynamic recrystallization mechanism during hot deformation of Incoloy 028 alloy. J Mater Sci Technol Res 2020;42:241–53.
[116] Fernee H, Nairn J, Atrens A. Cold worked Cu-Fe-Cr alloys. J. Mate. Sci 2001;36:5497–510.
[117] Guo FA, Xiang CJ, Yang CX, Cao XM, Mu SG, Tang YQ. Study of rare earth elements on the physical and mechanical properties of a Cu-Fe-P-Cr alloy. Mater. Sci. Eng. B 2008;147:1–6.
[118] Cao H, Min JY, Wu SD, Xian AP, Shang JK. Pinning of grain boundaries by second phase particles in equal-channel

angularly pressed Cu-Fe-P alloy. Mater. Sci. Eng. A 2006;431:86–91.
[119] Wang BJ, Zhang Y, Tian BH, Jia YL, Volinsky Alex A, Yakubovd V, et al. Nanoscale precipitates evolution and strengthening mechanism of the aged Cu-Mg-Fe-Sn-P-Y electrical contact wire. J. Mater. Res. Technol 2020;9(3):6352–9.
[120] He WJ, Chapuis A, Chen X, Liu Q. Effect of loading direction on the deformation and annealing behavior of a zirconium alloy. Mater. Sci. Eng. A 2018;734:364–73.
[121] Cheng WL, Bai Y, Ma SC, Wang LF, Wang HX, Yu H. Hot deformation behavior and workability characteristic of a fine-grained Mg-8Sn-2Zn-2Al alloy with processing map. J Mater Sci Technol 2019;35:1198–209.
[122] Wu YT, Liu YC, Li C, Xia XC, Huang Y, Li HJ, et al. Deformation behavior and processing maps of Ni3Al-based superalloy during isothermal hot compression. J Alloys Compd 2017;712:687–95.
[123] Srinivasan N, Prasad YVRK, Rama Rao P. Hot deformation behavior of Mg-3Al alloy-A study using processing map. Mater. Sci. Eng. A 2008;476:146–56.
[124] Ji GL, Li Q, Ding KY, Yang L, Li L. A physically-based constitutive model for high temperature deformation of Cu-0.36Cr-0.03Zr alloy. J Alloys Compd 2015;648:397–407.
[125] Wu YS, Liu Z, Qin XZ, Wang CS, Zhou LZ. Effect of initial state on hot deformation and dynamic recrystallization of Ni-Fe based alloy GH984G for steam boiler applications. J Alloys Compd 2019;795:370–84.
[126] Lu DP, Wang J, Zeng WJ, Liu Y, Lu L, Sun BD. Study on high-strength and high-conductivity Cu-Fe-P alloys. Mater. Sci. Eng. A 2006;421:254–9.
[127] Dong QY, Shen LN, Wang MP, Jia YL, Li Z, Cao F, et al. Microstructure and properties of Cu-2.3Fe-0.03P alloy during thermomechanical treatments. Trans. Nonferrous. Met. Soc. China 2015;25:1551–8.
[128] Dong QY, Shen LN, Cao F, Jia YL, Liao KJ, Wang MP. Effect of thermomechanical processing on the microstructure and properties of a Cu-Fe-P alloy. J Mater Eng Perform 2015;24:1531–9.
[129] Kim JM, Park JS, Kim KT. Electrical conductivity and tensile properties of severely cold-worked Cu-P based alloy sheets. Met. Mater. Int 2010;16:657–61.
[130] Wang DPLu J, Lu L, Liu Y, Xie SF, Sun BD. Effect of boron and cerium on microstructures and properties of Cu-Fe-P alloy. J. Rare. Earth 2006;24:602–6.
[131] Xiao XP, Xu H, Chen JS, Liang QM, Wang JF, Zhang JB. Aging properties and precipitates analysis of Cu-2.3Fe-0.03P alloy by thermomechanical treatments. Mater Res Express 2017;4:116511.
[132] Zhang J, Cui XC, Ma JK, Wang YH. Study of high-strength and high-conductivity Cu-Sn-Fe alloys. Mater. Sci. Poland 2016;34(1):142–7.
[133] An JC, Wang BJ, Zhang Y, Tian BH, Volinsky Alex A, Liu Y, et al. Mechanical and electrical properties and phase analysis of aged Cu-Mg-Ce alloy. J Mater Eng Perform 2020;29:1–9.
[134] Kim HG, Lee TW, Han SZ, Euh K, Kim WY, Lim SH. Microstructural study on effects of C-Alloying on Cu-Fe-P cast alloy. Met. Mater. Int 2012;18:335–9.
[135] Kim HG, Han SZ, Euh K, Lim SH. Effects of C addition and thermo-mechanical treatments on microstructures and properties of Cu-Fe-P alloys. Mater. Sci. Eng. A 2011;530:652–8.
[136] Choi JH. Aging behavior and precipitate analysis of copper-rich Cu-Fe-Mn-P alloy. Mater. Sci. Eng. A 2012;550:183–90.